JOURNAL OF PROPULSION AND POWER
Vol. 11, No. 6, November–December 1995

Three-Dimensional Navier–Stokes Heat Transfer Predictions for Turbine Blade Rows

R. J. Boyle*
NASA Lewis Research Center, Cleveland, Ohio 44135
and
P. W. Giel†
Sverdrup Technology, Inc., Cleveland, Ohio 44142

Results are shown for a three-dimensional Navier–Stokes analysis of both the flow and the surface heat transfer for four turbine blade rows. Heat transfer comparisons are made with the experimental shock-tunnel data of Dunn and Kim and with the data of Blair for the rotor of a large-scale rotating turbine. The analysis was done using the steady-state, three-dimensional, thin-layer Navier–Stokes code developed by Chima, which uses a multistage Runge–Kutta scheme with implicit residual smoothing. An algebraic mixing length turbulence model is used to calculate turbulent eddy viscosity. The variation in heat transfer due to variations in grid parameters is examined. The effects of rotation, tip clearance, and inlet boundary-layer thickness variation on the predicted blade and end-wall heat transfer are examined.

Nomenclature

C = chord
C_p = pressure coefficient $(P - P'_{IN})/(P'_{IN} - P_{EXIT})$
P = pressure
Re = unit Reynolds number
St = Stanton number based on inlet conditions
s = fractional surface distance
T = temperature
x = fractional chordwise distance
y = distance normal to surface
y^+ = normalized distance from surface
δ = full boundary-layer thickness
ν = kinematic viscosity
ρ = density

Subscripts
EXIT = blade row hub exit
g = gas total
IN = blade row inlet
w = wall
1 = first grid line from surface

Superscript
$'$ = total

Introduction

ACCURATE heat transfer predictions are needed in turbomachinery designs for advanced propulsion systems. Improved heat transfer prediction capability allows for reduced coolant requirements for given heat loads to the turbine blades. Alternately, improved heat transfer predictions would allow for an increase in turbine inlet temperature for a given amount of coolant. Even if the blades are uncooled, accurate predictions are needed to determine blade temperatures during transients, since these temperatures determine thermal stresses. Experimental data show three-dimensional heat transfer patterns on the blade and the end-wall surfaces.[1–7] These three-dimensional heat transfer patterns were observed in data from both cascade facilities and on rotating turbine blades. Blair[6] showed heat transfer on the rotor surface in the tip region nearly double that in the midspan region, indicating the importance of clearance in determining blade heat transfer. Two-dimensional heat transfer analyses are unsuitable for predicting end-wall heat transfer distributions and do not account for clearance effects. The three-dimensional nature of the experimental data show the need for three-dimensional heat transfer analyses.

Comparisons have been made between predicted and measured vane and rotor heat transfer using three-dimensional Navier–Stokes analyses,[8–10] typically for cases where neither tip clearance nor rotation were present. This article shows comparisons between predicted and measured heat transfer for individual blade rows of turbine stages. Comparisons are shown with the heat transfer data of Dunn and Kim,[7] and with the data of Blair.[6] Dunn and Kim measured vane and rotor heat transfer in a shock tunnel for the Space Shuttle Main Engine (SSME), high pressure fuel turbine (HPFT), operating at the design turbine pressure ratio. Measurements were made at three spanwise locations for the stator and rotor of the first stage and at midspan for the stator of the second stage. Blair measured heat transfer for the rotor of a low-speed turbine in a large-scale rotating rig over a range of Reynolds numbers and flow coefficients. Full span heat transfer data were obtained on both surfaces of the rotor and on the hub end-wall.

The heat transfer analysis was done using the steady-state three-dimensional analysis developed by Chima.[11,12] This is an explicit, finite difference, thin-layer Navier–Stokes analysis. An algebraic turbulence model is used to calculate the turbulent eddy viscosity. One question that arises with respect to the clearance flow region is the degree of detail needed for calculating the flow in the gap between the top of the rotating blade and the stationary shroud. It is possible to generate a grid for the region on top of the blade in this gap and a grid would be necessary to calculate the heat transfer on the top surface of the rotor. However, a simpler approach is to average the flow variables for the blade surface grid line

Presented as Paper 92-3068 at the AIAA/SAE/ASME/ASEE 28th Joint Propulsion Conference and Exhibit, Nashville, TN, July 6–8, 1992; received Oct. 23, 1992; revision received March 1, 1995; accepted for publication March 29, 1995.

*Aerospace Engineer, Internal Fluid Mechanics Division. Member AIAA.

†Lewis Research Center Group; currently, Senior Research Engineer, Turbomachinery Analysis Section, NYMA, Inc. Member AIAA.

when the grid is extended into the clearance region. Since part of the motivation for this work was to determine an efficient approach that gives accurate results, the simpler approach was used.

Description of Analysis

Details of the three-dimensional, thin-layer Navier–Stokes analysis used are found in works by Chima[11] and Chima and Yokota.[12] Briefly, the code, known as RVC3D, uses an explicit time-marching algorithm, employing implicit residual smoothing. A four-stage Runge–Kutta scheme was used. A spatially varying time step along with a Courant–Friedrichs–Lewy (CFL) number of 5 was used to speed convergence to the steady-state solution.

An analysis was done to determine if a simple, and therefore, relatively fast approach to tip clearance modeling would correctly predict the effect of clearance on rotor heat transfer. There is no grid in the clearance region above the rotor. However, in the gap between the rotor and the shroud the grid around the blade is extended outward to the shroud. In the clearance region the "wall" boundary conditions are modified. In this region a zero-slip wall boundary condition is not imposed, as it is imposed on the actual blade surface. Instead, the flow variables for the wall boundary in the clearance region are averaged between the pressure and suction surface. This averaging process results in a pressure gradient at the grid wall boundary in the clearance region. This pressure gradient induces flow through the clearance gap from the pressure to the suction surface.

The transition locations were calculated using the midspan transition criteria. The start of transition and the length of transition in terms of distance from the stagnation point were determined using the procedure described in Ref. 13 for the midspan flow conditions. As discussed in Ref. 13, the transition prediction used the procedure recommended by Mayle,[14] in which the transition location is a function of Reynolds number, freestream turbulence, and the blade passing frequency of the upstream blade row. In the course of this work the effects of variation in the turbulence model were examined. Changing the model resulted in different heat transfer levels. However, the same relative three-dimensional patterns were observed. A model was chosen for the three-dimensional heat transfer calculations and it is expected that other models would yield similar three-dimensional effects. The turbulence model employed near-wall damping and wall functions were not used. All cases were run with a specified wall temperature. A constant value of $Pr_t = 0.9$ was used to model the turbulent heat flux terms. The assumption of a constant turbulent Prandtl number is consistent with the relatively simple algebraic turbulence model used in the analysis and was shown by Boyle[18] to result in nearly the same heat transfer as a variable turbulent heat transfer model. Also, the near-wall variation of the turbulent Prandtl number is not well understood at this time.

C-type grids, which facilitate obtaining accurate flow and heat transfer solutions in the leading-edge region, were used. The leading-edge region is a region of high heat transfer on both the blade surface and on the end-wall in front of the blade. Grids were generated using the code Tcgrid developed at Lewis by Chima et al.[15] with the blade and end-wall geometry defined as in the Meridl program of Katsanis.[16] The Tcgrid program interpolates this information to generate input data for a relatively small number of two-dimensional blade-to-blade grids. The subroutine within the Tcgrid program that is used to generate these two-dimensional grids is based on Sorenson's Grape code.[17] After the blade-to-blade grids were generated, the resulting grids were interpolated to give grids for each spanwise grid plane.

When generating the grids it was necessary to determine the spacing of the first grid line from the surface. It is not the physical spacing y_1, but rather the normalized spacing y_1^+, that should be specified to obtain accurate heat transfer results. An a priori estimate of y^+ was calculated as given by Boyle,[18] except that the gas-to-wall temperature ratio was explicitly accounted for. The expression used for the reference y^+ is

$$y^+_{REF} = 0.17 y_1 Re^{0.9} (T_g/T_w)^{1.5}/C^{0.1} \quad (1)$$

The ratio T_g/T_w is important only when the gas total temperature to wall temperature ratio is large, as it was in some of these comparisons. An exponent of 1.5 was used to account for the effect of temperature on both density and viscosity. The temperature ratio term was included because it improved the agreement between the y^+_{REF} used in generating the grid, and the maximum value of y_1^+ calculated from the Navier–Stokes solution. In all of the cases presented the spacing of the first grid line from the hub and shroud was maintained at the same value as the spacing of the first grid line from the blade.

Results and Discussion

Because of the relatively long computational times involved in three-dimensional Navier–Stokes calculations, it is necessary to determine the smallest grid size that results in accurate predictions. First, the grid size parameters and the near-wall spacing, along with the end-wall boundary thickness, will be examined to show their relative importance in calculating accurate turbine blade heat transfer. Next, the heat transfer and pressure distribution comparisons with experimental data will be made for the individual blade rows.

Grid Parameter Results

The first-stage stator of the SSME high-pressure fuel turbine was used to determine the appropriate grid parameters. The flow conditions are those of the low Reynolds number case of Dunn and Kim.[7] The grid sensitivity study was done assuming fully turbulent flow. Figure 1 shows the geometry and a typical grid used for the heat transfer predictions, with the grid clustered near each of the solid walls. The chord is shorter at the hub than at midspan, which results in an underturning of the flow at the hub. Figure 2 shows the effects of grid parameters primarily on Stanton number, but also on the surface pressure distribution, and on the calculated value of y_1^+. Results are shown for a combination of five different grids, and Table 1 summarizes the parameters for the different grids.

Table 1 Characteristics of first-stage stator grids

Grid	A	B	C	D	E
Streamwise number	214	145	145	145	145
Pitchwise number	43	43	43	43	43
Spanwise number	43	43	65	65	65
y^+_{REF}	2.3	2.3	1.2	2.3	2.3

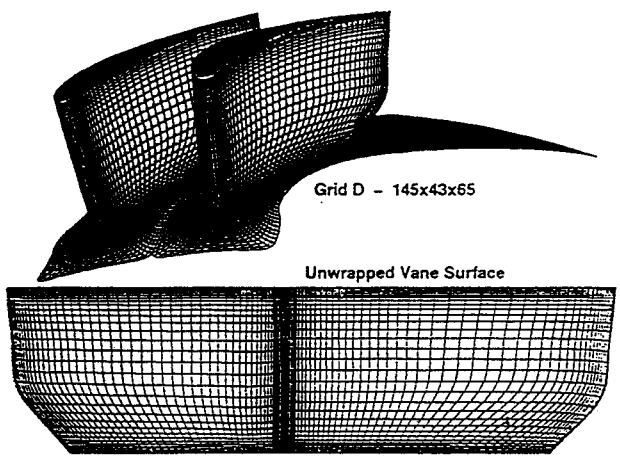

Fig. 1 Geometry—stator 1.

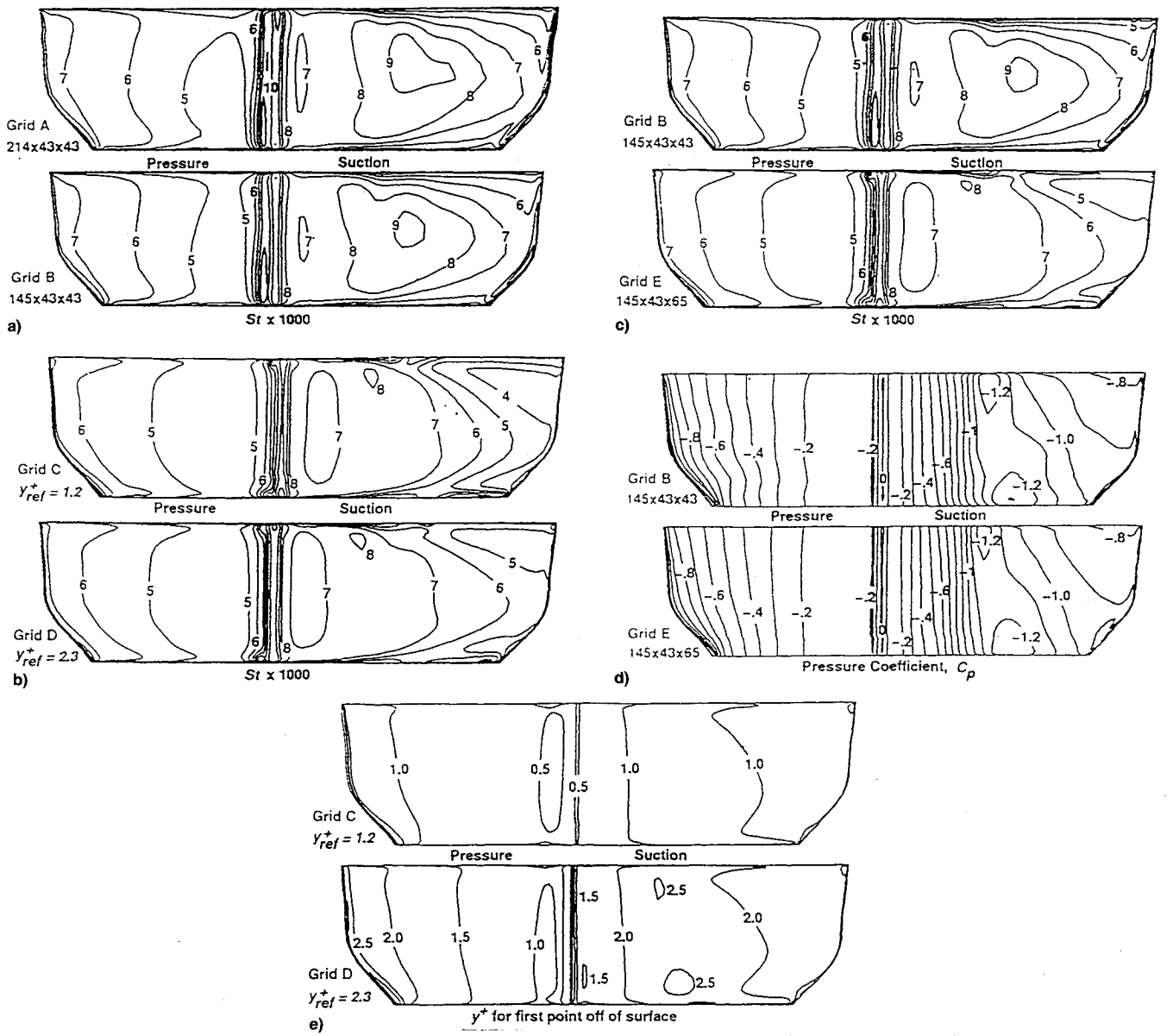

Fig. 2 a) Effects of streamwise grid density on vane heat transfer, b) effects of near-wall grid spacing on vane heat transfer, c) effects of spanwise grid stretching on vane heat transfer, d) effects of spanwise grid stretching on vane surface pressure, and e) variation of y^+ with near-wall grid spacing.

The choice of grid parameters was influenced by the grid sensitivity results presented by Boyle[18] for a two-dimensional Navier–Stokes heat transfer analysis. Note that grids D and E were generated with different grid input parameters, which resulted in locally different grids. These two grids differed in terms of grid spacing around the blade and in orthogonality to the vane surface, but had the same number of grid lines and near-wall spacing. Both were felt to be acceptable grids, but neither was felt to be superior to the other in an overall sense.

Figure 2a shows Stanton number results for two cases that differ in the number of streamwise grids by comparing grids A and B. The number of streamwise grids is the total number of grid lines that extend out from the blade surface or from the C-grid cut line in the wake region. Grid A had 214 streamwise grid lines, of which 68 were in the wake; grid B had 145 streamwise grid lines, of which 40 were in the wake. The coarser grid with 145 lines had nearly the same Stanton number distribution as the finer grid, showing that a relatively sparse grid could be used around the blade for the heat transfer predictions.

Figure 2b shows the effect of varying the near-wall spacing on Stanton number using grids C and D. Increasing y^+_{REF} from 1.2 to 2.3 had little effect on the blade surface Stanton number. Calculations with the smaller y^+_{REF} resulted in appreciably different heat transfer rates only in the suction surface trailing-edge region.

Figure 2c shows the effect on the Stanton number of grid stretching in the spanwise direction. Grids B and E, used for the comparisons, had the same spacing for the first grid line off each end-wall. Because grid B had only 43 spanwise grid lines it was stretched considerably more. The ratio of Δy_2 to Δy_1 was 1.6 for grid B and this ratio was 1.3 for grid E. Δy is the distance between adjacent grid lines in the radial direction, with Δy_1 being the distance between the hub or tip and the first grid line off the wall. The effect of grid stretching is very noticeable on vane surface heat transfer. This is somewhat surprising since the grid variation is only in the spanwise direction and not in a direction normal to the blade. The span-to-pitch ratio for this case is 1.1, so that the grid outward from the blade was stretched about the same as grid E was stretched in the spanwise direction. With C-type grids, the

grid extends from the blade surface only to the midchannel and there is no clustering near the midchannel. The same number of lines in the spanwise and blade-normal directions results in far greater stretching in the spanwise directions for all but very low span-to-pitch ratios.

Generating grids for turbine blade geometries involves compromises. Because of the highly turned geometry, no one grid is optimum over the entire flowfield. Sensitivity of heat transfer to choice of grid optimization can be seen by comparing results in Figs. 2b and 2c for the same grid parameters. The Stanton number results do not differ significantly between grid D in Fig. 2b and grid E in Fig. 2c.

Figure 2d shows the effect on surface pressures comparing grids B and E. The differences are smaller than one might expect based on the differences in the surface heat transfer. These almost contradictory results suggest that the heat transfer is influenced by the analysis's ability to calculate the secondary flows across the end-wall.

Figure 2e shows calculated y_1^+ values on the blade surface for grids C and D. For both values of y^+_{REF} the maximum value calculated from the Navier–Stokes analysis is only slightly in excess of the a priori estimate given by Eq. (1). Because this example is for a gas-to-wall temperature ratio of 1.9, neglecting the gas-to-wall temperature ratio term in calculating y^+_{REF} would reduce the value by nearly a factor of 3. If the gas-to-wall temperature ratio term was neglected in calculating y^+_{REF}, the value of y^+_{REF} would be significantly less than the maximum value of y^+ calculated using the Navier–Stokes analysis.

Grids of 400,000 points took approximately 2.5 s of CPU time on a Cray Y-MP computer per iteration. Typically, heat transfer converged within 2500 iterations, even if not initialized with a similar flowfield. Less than 8 MW of core were required for this number of grid points. Both maximum and L_2 norm continuity equation residuals typically reduced three orders of magnitude within 3000 iterations. This reduction in residuals was sufficient, since no change in the surface heat transfer was observed over the last 500 iterations. Figure 3 shows the residual history and the variation in exit conditions as a function of iteration number for grid C. The convergence rate for grid C was about two-thirds of the rate for the other grids, probably because grid C had the smallest near-wall spacing.

Figure 4 shows the effect of grid stretching on the end-wall heat transfer. After examining the results shown in Fig. 2c it is not surprising that this effect is very large. Viewing these differences as uncertainties in comparisons with experimental measurements shows that coarse spanwise grids result in unacceptable computational errors. The strong sensitivity of the heat transfer to grid stretching, coupled with the relatively weak sensitivity to the near-wall spacing, suggest that the effect of trading increased near-wall spacing for reduced stretching be further examined.

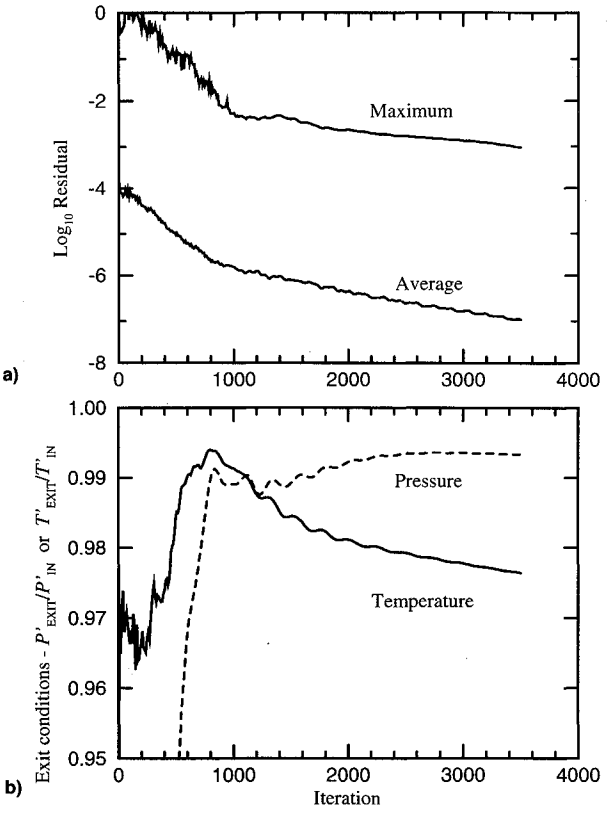

Fig. 3 Computational convergence history, grid C: a) residuals and b) exit flow properties.

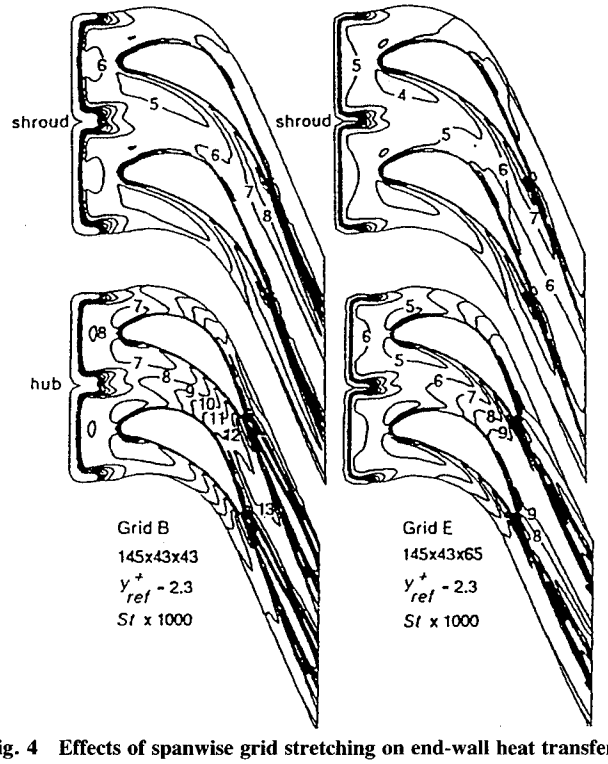

Fig. 4 Effects of spanwise grid stretching on end-wall heat transfer.

Inlet Boundary-Layer Effect

Figure 5 shows the blade and end-wall heat transfer assuming an inlet boundary layer on each end-wall equal to 30% of the full span. This inlet boundary-layer thickness was chosen arbitrarily large to illustrate its effect on blade and end-wall heat transfer. Inlet boundary-layer thicknesses of the same order as 30% of span have been reported measured in end-wall heat transfer experiments.[1,4] While the effect of an inlet boundary layer on the heat transfer distribution is not as great as the effect of grid stretching, this effect is noticeable. If a boundary layer is present in the test, it should be included in the analysis.

Experimental Data Comparisons

Figure 6a compares predicted surface pressures with the data of Hudson et al.[19] taken at the NASA Marshall Space Flight Center (MSFC) turbine test facility. It was felt to be appropriate to compare surface pressure results with the data taken in the MSFC blowdown facility, because the tests in this facility were aimed at obtaining accurate steady-state surface pressures. Data are shown at 10, 50, and 90% of span. The Navier–Stokes analysis considers only an isolated blade row. The inlet total pressure and blade row pressure ratio for this and subsequent blade rows were obtained from the quasi-three-dimensional flow analysis code MTSB.[20] The analysis

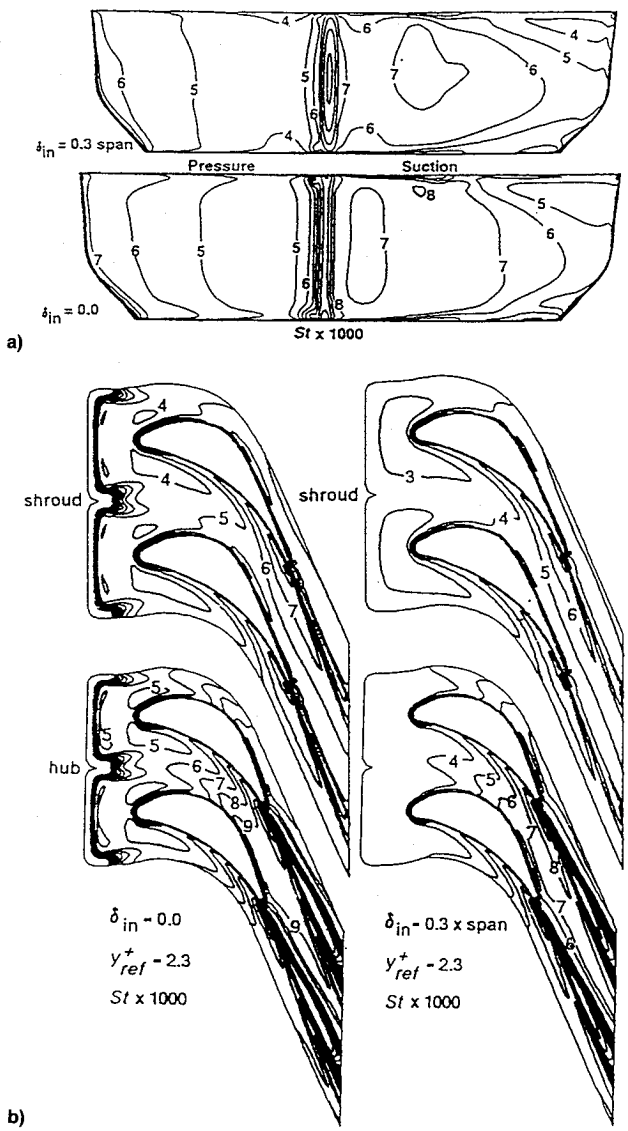

Fig. 5 Effects of inlet boundary layer on a) vane heat transfer and b) end-wall heat transfer.

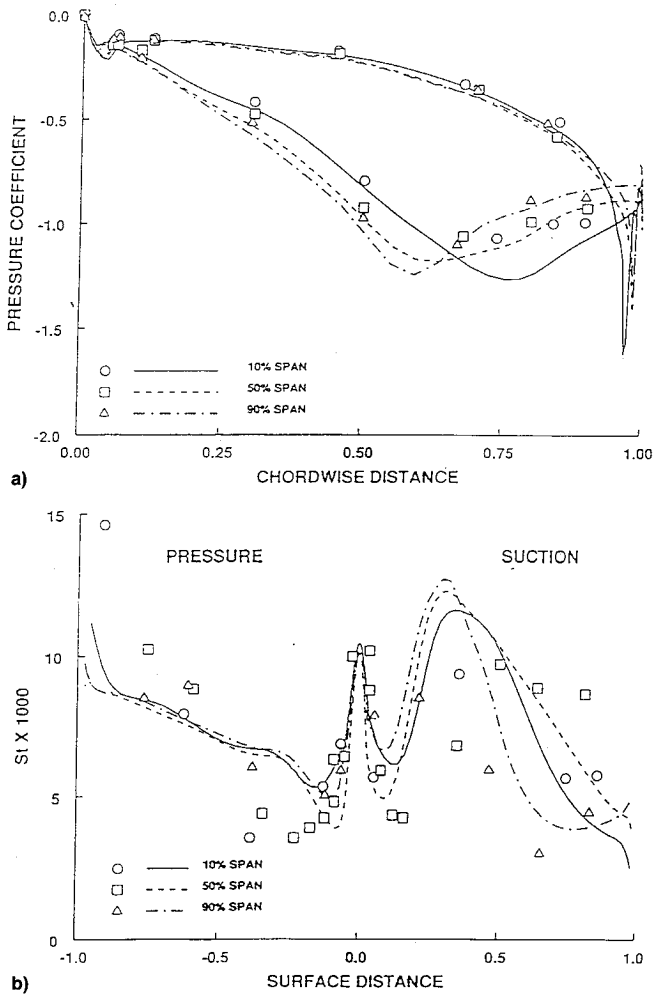

Fig. 6 Stator 1 a) pressure distribution[19] and b) heat transfer.[7]

was done for the same two-stage turbine pressure ratio as the experiments. The Navier–Stokes analysis predicted the surface pressures at 50 and 90% of span reasonably well, but did not do as well at 10% of span. This may have been due to the circumferential nonuniformity of the stator cutback. The analysis was done for the average cutback at the hub, but the nonuniformity might have affected the 10% span surface pressures.

Figure 6b shows heat transfer comparisons for the low Reynolds number for the data from Dunn and Kim.[7] Comparisons are shown for the low Reynolds number cases so as to minimize uncertainties associated with grid spacing. Experimental Stanton numbers for all blade rows of the SSME fuel turbine were based on the first stator inlet density and velocity and the predicted Stanton numbers were calculated accordingly. An inlet boundary-layer thickness of 8% of span was used for each end-wall based on the flow and geometry upstream of the stator. At midspan the analysis is in reasonably good agreement with the experimental data. For both pressure and suction surfaces the data indicate a longer transition length than was used in the analysis. This would account for the overprediction of the Stanton number near a third of the suction surface distance. The analysis is in reasonably good agreement with the data for the rearward portion of the pressure surface and both show little spanwise variation in heat transfer. On the suction surface the analysis agrees reasonably well with the data in the fully turbulent region at 10, 50, and 90% of span. The results in this figure, along with those presented in Fig. 2, are further indications of the importance of spanwise stretching. The results in Fig. 2c show lower heat transfer at 10 and 90% of span in the rearward portion of the suction surface for the finer spanwise grid. The finer spanwise grid was necessary to predict the spanwise variation in heat transfer. For the surface pressures the poorest agreement was at 10% of span, where the heat transfer agreement is nearly the same as at midspan.

Figure 7 shows the predicted heat transfer for the first stage rotor of the SSME high-pressure fuel turbine. The analysis was done assuming a smooth blade surface based on the analysis presented in Ref. 18, which concluded that the blades are hydraulically smooth at this Reynolds number. Heat transfer distributions are shown on both the unwrapped surface of the rotor and on the hub end-wall. The analysis was done using a 145 × 40 × 65 grid, with a y^+_{REF} of 2, and a rotor tip clearance of 2.2% of span. The inlet radial profile for the rotor analysis was obtained using the circumferential average of the stator exit results. The highest end-wall heat transfer occurs just in front of the leading edge and is very localized. The second highest heat transfer in the blade region is in the throat region. Dunn and Kim[7] gave two measurements of end-wall Stanton numbers. The values were 0.0065 and 0.007 at 20% and 60% of the rotor chord, respectively.

Figure 8 compares predicted and measured heat transfer at 10, 50, and 90% of span. The analysis underpredicts the leading-edge heat transfer, but this was expected since the turbulence model did not account for any augmentation in heat

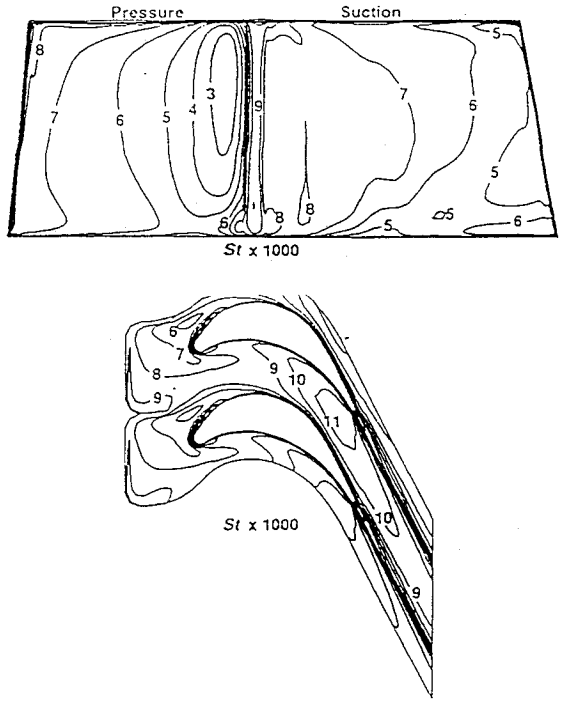

Fig. 7 Rotor 1 heat transfer prediction with clearance: a) unwrapped rotor surface and b) hub surface.

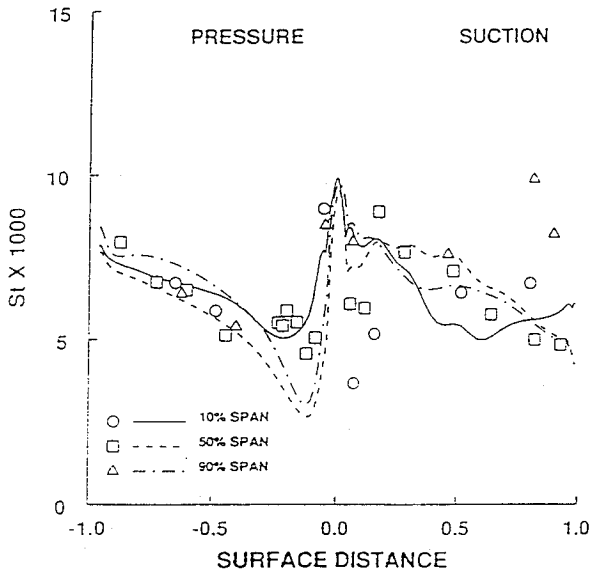

Fig. 8 Rotor 1 heat transfer.[7]

transfer due to freestream turbulence prior to transition. Depending on the correlation used, an increase in the leading-edge heat transfer of up to 40% could be expected. The predicted heat transfer agrees well with the experimental data along the pressure surface. On the suction surface the analysis agrees well with the data, except in the transition region, and near the trailing edge at 90% of span. The disagreement with the data in the transition region may not be the fault of the transition model, but rather the defining of stagnation points from which boundary layers are calculated to determine the start of transition. In a three-dimensional flowfield there are ambiguities associated with the determination of the stagnation line. The analysis shows a smaller variation in heat transfer between 50–90% of span than the experimental data. However, in the clearance model there is no flow resistance at the top of the blade and this assumption would result in higher than actual flow in the tip region.

To better understand the behavior of the calculations it is useful to show results for different assumptions; comparing results for the different assumptions should clarify the factors determining the heat transfer. Figure 9 shows the blade heat transfer assuming a shrouded rotor. The outer casing rotates with the rotor and there is no clearance gap. These results can be compared with those shown in Fig. 7. Close to the trailing edge on the suction side the heat transfer is higher without clearance. Everywhere else in the tip region the Stanton number is lower when there is no clearance. Based on these data alone the assumption made for flows in the clearance gap appears to underestimate the effect of tip clearance, does give the correct trend in heat transfer.

Figure 10 shows the vane surface Stanton numbers for the second-stage stator. This stator is similar to the first-stage stator, but there is no cutback at the trailing edge. The heat transfer is similar to that for the first-stage vane. The three-dimensional effects on the vane heat transfer are noticeable and show greater spanwise symmetry than for the first vane. This result is essentially due to the absence of the cutback for the second-stage vane. Figure 11a compares predicted pressure distributions at 10, 50, and 90% span with the data of Hudson et al.[19] Here, the prediction agrees better with the data than for the pressure distribution for the first-stage vane. The absence of a nonuniform cutback probably accounts for the better agreement with the data for the second-stage vane, compared to the first stage vane. Since the second stator has no cutback, there is less passage-to-passage variation in its exiting flowfield. Figure 11b compares midspan heat transfer predictions with the data of Dunn and Kim.[7] Near the leading edge, as expected, the predicted heat transfer is lower than measured. In the leading-edge region it was expected that the analysis would underpredict the heat transfer rates, since the analysis did not account for heat transfer augmentation due to the high turbulence levels generated by the passing of the wakes of the upstream blade rows. Elsewhere on the vane, the analysis overpredicts the blade surface heat transfer. The analysis predicted transition to occur close to the leading edge for the suction surface. However, the data indicate that transition was supressed for most of the suction surface.

Figure 12 shows the rotor surface heat transfer comparisons for a low Reynolds number case with the data of Blair. The analysis was done with a 145 × 40 × 65 grid. The rectangular shape of the unwrapped blade plot is the result of using a normalized surface distance consistent with that used by Blair. Comparisons for the suction and pressure surfaces show that in both the predictions and experimental data there are very

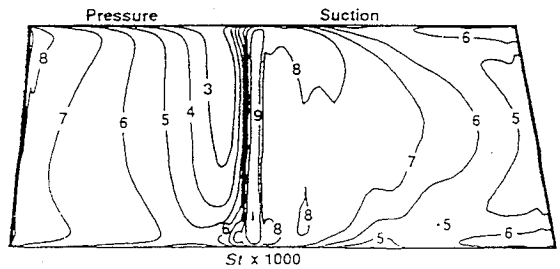

Fig. 9 Rotor 1 heat transfer calculation. Zero clearance, rotating shroud.

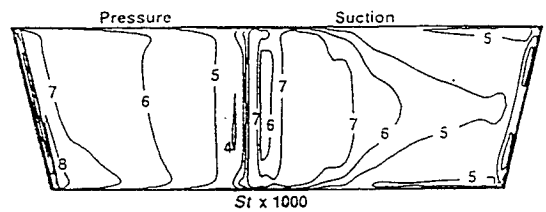

Fig. 10 Stator 2 heat transfer prediction.

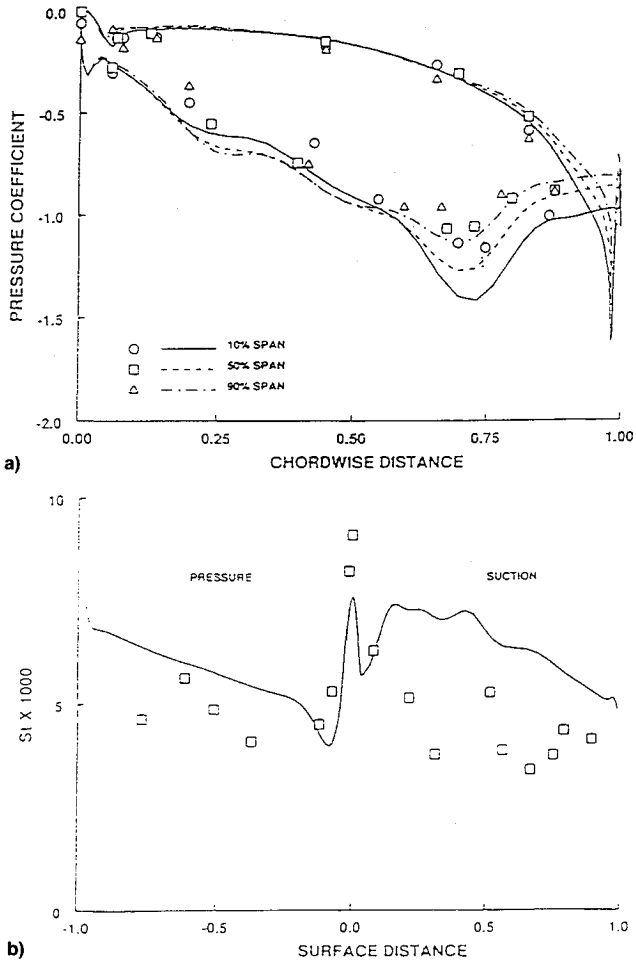

Fig. 11 Stator 2 a) pressure distribution[19] and b) midspan heat transfer.[7]

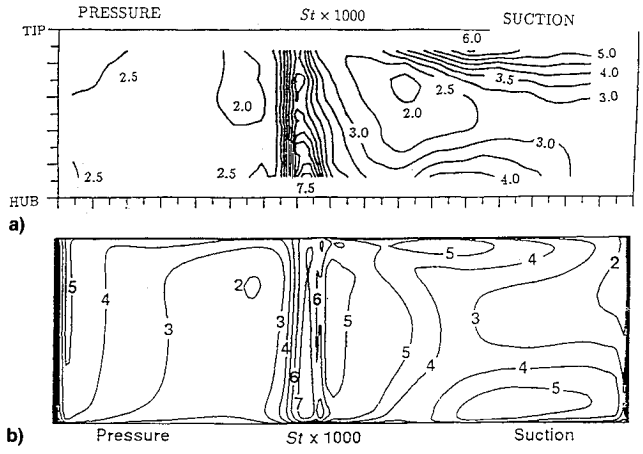

Fig. 12 Comparison of predicted and measured rotor surface heat transfer, $Re = 2.37 \times 10^5$: a) design flow angles and b) prediction, 1% clearance.

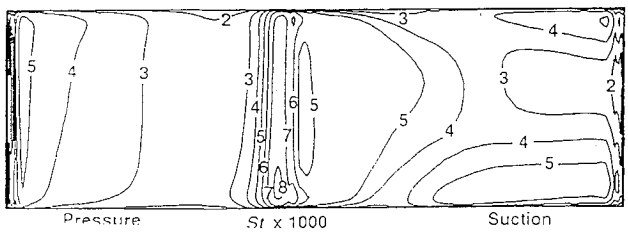

Fig. 13 Calculated heat transfer for Blair's rotor, zero clearance, and rotating shroud.

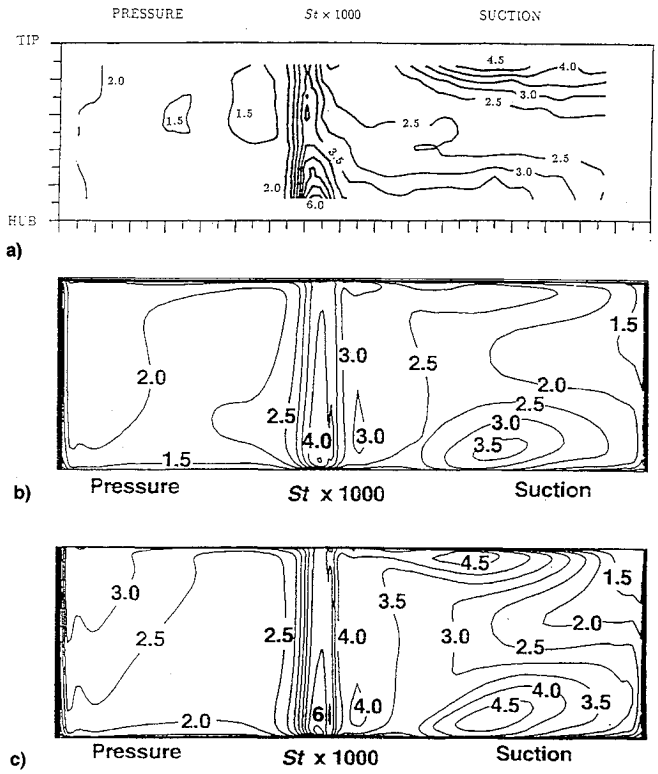

Fig. 14 Spanwise grid density effects on predicted heat transfer, and comparison with data of Blair,[6] $Re = 5.838 \times 10^5$: a) design flow angles, b) prediction; 1% clearance, 145 × 40 × 65; and c) prediction, 1% clearance, 145 × 40 × 85.

high heat transfer rates in the tip region on the suction surface. Because this high heat transfer is in the tip region, one is likely to assume that this high heat transfer is the result of clearance flows. However, it should be noted that there is high heat transfer in the hub region at almost the same surface distance. The suction surface heat transfer in the hub region is higher than at midspan, but not as high as in the tip region. The analysis correctly predicts this three-dimensional pattern. Figure 13 shows a calculation for the same conditions as the prediction in Fig. 12, except that there is no clearance and the shroud rotates with the rotor. In the tip region the suction surface heat transfer is significantly lower than in Fig. 12, showing the relative importance of these phenomena.

Figure 14 shows a comparison of the predicted blade surface heat transfer with the experimental data of Blair for a high Reynolds number case. Predictions are shown for two grids with 65 and 85 lines in the spanwise direction, respectively. In contrast with the results in Fig. 12 for the low Reynolds number case, predictions with only 65 spanwise grid lines did not show high heat transfer on the suction surface in the region near the tip. However, there was a significant improvement in the degree of agreement with the data when 85 spanwise grid lines were used.

Conclusions

The results of this work showed that a three-dimensional thin-layer Navier–Stokes analysis was able to predict heat transfer with reasonable accuracy. This result was true for cases with and without rotation. A relatively simple, and therefore, computationally efficient, tip clearance model gave useful results. This model resulted in good agreement with experimental data with respect to the heat transfer on the surfaces of the blade in the tip region for the data of Blair, but underpredicted the tip clearance effect for the data of Dunn and Kim. However, this model, in which the flow variables were averaged at the extended surface of the blade in

the tip region, gives no information with respect to the heat transfer on the tip surface of the blade. Nonetheless, it is a useful tool for three-dimensional heat transfer analysis, and this approach warrants further investigation.

Grid sensitivity studies showed that heat transfer was most sensitive to the grid stretching. Both blade and end-wall heat transfer were highly dependent on spanwise grid stretching. Heat transfer was more sensitive to this parameter than to variations in near-wall spacing, streamwise grid density, or local optimization of the grid. These results show that, while it is desirable to maintain a close near-wall spacing, this parameter might be relaxed in favor of less grid stretching in the interest of obtaining accurate and economical heat transfer predictions.

The results of the analysis showed that in a multiblade row analysis, the results of the upstream calculation should be used as the inlet condition for successive blade rows. Because of the relative motion of the blade rows, circumferential averaging of the flow variables was done. Although the averaging does not completely preserve the flowfield, the boundary layers on the end-walls are maintained between blade rows.

References

[1]Graziani, R. A., Blair, M. F., Taylor, J. R., and Mayle, R. E., "An Experimental Study of Endwall and Airfoil Surface Heat Transfer in a Large Scale Turbine Blade Cascade," *Journal of Engineering for Power*, Vol. 102, No. 2, 1980, pp. 257–267.

[2]Blair, M. F., "An Experimental Study of Heat Transfer and Film Cooling in Large-Scale Turbine Endwalls," *Journal of Heat Transfer*, Vol. 96, No. 2, 1974, pp. 525–529.

[3]York, R. E., Hylton, L. D., and Mihelc, M. S., "Experimental Endwall Heat Transfer and Aerodynamics in a Linear Vane Cascade," *Journal of Engineering for Gas Turbines and Power*, Vol. 106, No. 1, 1984, pp. 159–167.

[4]Boyle, R. J., and Russell, L. M., "An Experimental Determination of Stator Endwall Heat Transfer," *Journal of Turbomachinery*, Vol. 112, No. 3, 1990, pp. 547–558.

[5]Blair, M. F., "An Experimental Study of Heat Transfer in a Large-Scale Turbine Rotor Passage," *Journal of Turbomachinery*, Vol. 116, No. 1, 1994, pp. 1–13.

[6]Blair, M. F., "The Effects of Reynolds Number, Rotor Incidence Angle, and Surface Roughness on the Heat Transfer Distribution in a Large-Scale Turbine Rotor Passage," United Technologies Research Center (UTRC) Rept. R91-970057-3, Nov. 1991.

[7]Dunn, M. G., and Kim, J., "Heat Transfer and Pressure Measurements and Comparison with Prediction for the SSME Two Stage Turbine," Calspan-Univ. of Buffalo Research Center (CUBRC) Rept. 640I, March 1992.

[8]Hah, C., "Numerical Study of Three-Dimensional Flow and Heat Transfer Near the Endwall of a Turbine Blade Row," AIAA Paper 89-1689, June 1989.

[9]Ameri, A. A., and Arnone, A., "Three Dimensional Navier-Stokes Analysis of Turbine Passage Heat Transfer," AIAA Paper 91-2241, June 1991.

[10]Choi, D., and Knight, C. J., "Computation of 3D Viscous Linear Cascade Flows," *AIAA Journal*, Vol. 26, No. 12, 1988, pp. 1477–1482.

[11]Chima, R. V., "Viscous Three-Dimensional Calculations of Transonic Fan Performance," AGARD Propulsion and Energetics Symposium on Computational Fluid Mechanics for Propulsion, San Antonio, TX, May 1991.

[12]Chima, R. V., and Yokota, J. W., "Numerical Analysis of Three-Dimensional Viscous Internal Flows," AIAA Paper 88-3522, June 1988; also NASA TM100878, 1988.

[13]Dunn, M. G., Kim, J., Civinskas, K. C., and Boyle, R. J., "Time-Averaged Heat Transfer and Pressure Measurements and Comparison with Prediction for a Two-Stage Turbine," *Journal of Turbomachinery*, Vol. 116, No. 1, 1994, pp. 14–22.

[14]Mayle, R. E., "The Role of Laminar-Turbulent Transition in Gas Turbine Engines," *Journal of Turbomachinery*, Vol. 113, Oct. 1991, pp. 509–537.

[15]Chima, R. V., personal communication, NASA Lewis Research Center, Cleveland, OH.

[16]Katsanis, T., and McNally, W. D., "Revised FORTRAN Program for Calculating Velocities and Streamlines on the Hub-Shroud Midchannel Stream Surface of an Axial-, Radial-, or Mixed-Flow Turbomachine or Annular Duct, Vol. I—User's Manual," NASA TN D-8430, March 1977.

[17]Sorenson, R. L., "A Computer Program to Generate Two-Dimensional Grids About Airfoils and Other Shapes by the Use of Poisson's Equation," NASA TM-81198, May 1980.

[18]Boyle, R. J., "Navier-Stokes Analysis of Turbine Blade Heat Transfer," *Journal of Turbomachinery*, Vol. 113, July 1991, pp. 392–403.

[19]Hudson, S. T., Gaddis, S. W., Johnson, P. D., and Boynton, J. L., "Cold Flow Testing of the Space Shuttle Main Engine High Pressure Fuel Turbine Model," AIAA Paper 91-2503, June 1991.

[20]Boyle, R. J., Haas, J. E., and Katsanis, T., "Predicted Turbine Stage Performance Using Quasi-Three-Dimensional and Boundary Layer Analyses," *Journal of Propulsion and Power*, Vol. 1, No. 3, 1985, pp. 242–251.